UC San Diego
UC San Diego Previously Published Works

Title

NitroSynapsin ameliorates hypersynchronous neural network activity in Alzheimer hiPSC models

Permalink

https://escholarship.org/uc/item/7m63w1d3

Journal

Molecular Psychiatry, 26(10)

ISSN

1359-4184

Authors

Ghatak, Swagata
Dolatabadi, Nima
Gao, Richard
et al.

Publication Date

2021-10-01

DOI

10.1038/s41380-020-0776-7

Peer reviewed

NitroSynapsin ameliorates hypersynchronous neural network activity in Alzheimer hiPSC models

Swagata Ghatak[1,2], **Nima Dolatabadi**[1,2], **Richard Gao**[3], **Yin Wu**[1], **Henry Scott**[1], **Dorit Trudler**[1,2], **Abdullah Sultan**[2], **Rajesh Ambasudhan**[1,2], **Tomohiro Nakamura**[1], **Eliezer Masliah**[4,5,*], **Maria Talantova**[1,2], **Bradley Voytek**[3,5,6], **Stuart A. Lipton**[1,2,5,†]

[1]Neuroscience Translational Center and Department of Molecular Medicine, The Scripps Research Institute, La Jolla, CA 92037, USA;

[2]Neurodegenerative Disease Center, Scintillon Institute, San Diego, CA 92121, USA;

[3]Cognitive Science, University of California, San Diego, La Jolla, CA 92093, USA;

[4]Department of Pathology, University of California, San Diego, La Jolla, CA 92093, USA;

[5]Department of Neurosciences, University of California, San Diego, School of Medicine, La Jolla, CA 92093, USA;

[6]Kavli Institute of Brain and Mind and Halicioglu Data Science Institute, University of California, San Diego, La Jolla, CA 92093, USA.

Abstract

Beginning at early stages, human Alzheimer's disease (AD) brains manifest hyperexcitability, contributing to subsequent extensive synapse loss, which has been linked to cognitive dysfunction. No current therapy for AD is disease-modifying. Part of the problem with AD drug discovery is that transgenic mouse models have been poor predictors of potential human treatment. While it is undoubtedly important to test drugs in these animal models, additional evidence for drug efficacy in a human context might improve our chances of success. Accordingly, in order to test drugs in a human context, we have developed a platform of physiological assays using patch-clamp electrophysiology, calcium imaging, and multielectrode array (MEA) experiments on human (h)iPSC-derived 2D cortical neuronal cultures and 3D cerebral organoids. We compare hiPSCs bearing familial AD mutations vs. their wild-type (WT) isogenic controls in order to

[†] Corresponding Author: Stuart A. Lipton, MD, PhD, Scripps Research, 11119 North Torrey Pines Road, Suite 125, La Jolla, CA 92037, USA. Phone Number: (858) 242-1385; Fax number: (858) 242-1384; slipton@scripps.edu.
[*]Present Address: National Institute on Aging, NIH, Bethesda, MD 20892, USA.

characterize the aberrant electrical activity in such a human context. Here, we show that these AD neuronal cultures and organoids manifest increased spontaneous action potentials, slow oscillatory events (~1 Hz), and hypersynchronous network activity. Importantly, the dual-allosteric NMDAR antagonist NitroSynapsin, but not the FDA-approved drug memantine, abrogated this hyperactivity. We propose a novel model of synaptic plasticity in which aberrant neural networks are rebalanced by NitroSynapsin. We propose that hiPSC models may be useful for screening drugs to treat hyperexcitability and related synaptic damage in AD.

Introduction

In human brains, neuronal hyperactivity is an early phenotype of Alzheimer's disease (AD), contributing to memory impairment and cognitive decline. Both sporadic (S) and familial (F) AD patients show aberrant, hypersynchronous electrical activity at the initial stages of the disease [1, 2]. Early-onset FAD, caused by genetic mutations in presenilin (PSEN or PS) 1/2 or amyloid precursor protein (APP) genes, increases amyloid-β (Aβ) peptide levels, which have been shown to contribute to hyperexcitability in cortical and hippocampal circuits [3–5]. FAD patients also show an increased propensity for seizures [6]. Moreover, both AD transgenic mouse models and human SAD patients manifest synaptic dysfunction leading to epileptic discharges [7–9].

While AD transgenic animal models have proven useful in studying important aspects of the disease, alone they have been of little predictive value in testing potential therapeutics for humans [10]. In part, this may have occurred because drugs often exhibit unique properties when tested on a human genetic background [10, 11]. Therefore, in the present study, we study the effects of potential therapeutic drugs on human induced pluripotent stem cell (hiPSC)-derived neurons in order to monitor pathophysiologically-relevant phenotypes in a 'human context.' We do this in the presence of AD patient-specific genetic mutations in these hiPSC-derived neurons vs. wild-type (WT) isogenic controls. Along these lines, we recently showed AD hiPSC-derived neuronal cultures and cerebral organoids compared to isogenic controls manifest ion channel dysfunction, dystrophic neurites, and synaptic damage in the face of elevated levels of Aβ in many ways similar to human AD brain [12]. Thus, these hiPSC-based models complement those provided by AD transgenic mice. Based on our results, we propose that concordance between transgenic mouse and hiPSC-based models in proper disease context may provide a more sound basis for moving forward with a novel therapeutic toward human clinical trials.

Although reductionist preparations such as hiPSC-based cultures may not be able to replicate every feature of the abnormal circuits in AD brains, our 2D neuronal cultures and 3D cerebral organoids contain both excitatory cerebrocortical neurons and inhibitory interneurons, and our cerebral organoids manifest cortical-like layer formation. Both our 2D neuronal cultures and 3D cerebral organoids exhibit neural network activity. For example, the hiPSC-derived neurons display slow (theta range) oscillations [12], which are known to spatially and temporally modulate cortical interactions as the travelling waves of the human cortex [13]. Furthermore, we observe similar network abnormalities as have been described in human AD brain EEGs in both our AD hiPSC-derived neuronal cultures and cerebral

organoids with regard to aberrant excitatory bursting, hypersynchronicity, and increased slow spontaneous fluctuations [14–16].

In terms of potentially treating this abnormal electrical activity in AD brains, prior studies have shown that hyperactivity of extrasynaptic NMDA-type glutamate receptors (eNMDARs) plays a critical role in synaptic damage in Alzheimer's disease [5, 17]. The aminoadamantane compound, memantine, is an uncompetitive, fast-off rate NMDAR antagonist, is an FDA approved drug for AD that acts as an open channel-blocker of NMDAR-associated channels, thus inhibiting excessive eNMDAR activation to some degree [18–20]. However, memantine has limited symptomatic effects on the disease. Therefore, our group developed a dramatically improved derivative of memantine designated NitroSynapsin (a.k.a YQW-036 in a series of drugs known as NitroMemantines) [5, 18, 21]. NitroSynapsin is a chemical adduct between an aminoadamantane moiety and a nitro group. Unlike memantine, NitroSynapsin acts as a dual-allosteric antagonist of eNMDARs, with the aminoadamantane, which binds in the ion channel, serving to target the nitro group to redox-modulatory/inhibitory sites on the extracellular surface of the receptor via S-nitrosylation. In animal models, the new dual functional drug is dramatically more efficacious than memantine in protecting synapses from neurodegenerative insult, providing synaptic protection virtually to control levels after a three-month treatment in the 3xTg AD transgenic mouse model [5, 18].

Nonetheless, heretofore it was not known whether NitroSynapsin could decrease the hypersynchronous neural network activity that has been associated with seizures and synaptic damage in a human context. Therefore, in the present study, we examined the effect of NitroSynapsin on these parameters in hiPSC lines bearing AD-related mutations.

Materials and methods

hiPSC lines used in this study

We used PSEN1 M146V/WT and APP^{swe}/WT hiPSC lines and the associated WT isogenic control [22], as well as the PSEN1 ΔE9/WT-hiPSC line and its WT isogenic control [23]. HiPSC lines were authenticated by DNA sequencing using primer sequences supplied by the laboratories generating these lines. The hiPSC lines were regularly tested for mycoplasma contamination using MycoAlert Plus kit (Lonza) and tested negative in each instance.

hiPSC maintenance and differentiation

Differentiation of hiPSCs was performed using standard protocols for generating cerebrocortical neurons [5]. Briefly, feeder-free hiPSCs cultured on Matrigel in mTeSR 1 medium (StemCell Technologies) were induced to differentiate by exposure for one week to a cocktail of small molecules: 2 μM each of A83–01, Dorsomorphin, and PNU74654 in DMEM/F12 medium supplemented with 20% Knock Out Serum Replacement (Invitrogen). Cells were then scraped manually to form PAX6$^+$ neurospheres and maintained for 2 weeks in DMEM/F12 medium supplemented with N2 and B27 (Invitrogen) and 20 ng ml^{-1} of basic FGF (R&D Systems). Subsequently neurospheres were seeded on polyornithine/laminin-coated dishes to form rosettes of human neural progenitor cells (hNPCs) that were manually

picked and expanded. For terminal differentiation into neurons, a 1:1 ratio of hNPCs and neonatal mouse astrocytes were seeded onto polyornithine/laminin-coated glass coverslips in DMEM/F12 medium supplemented with B27, N2, GDNF (20 ng ml^{-1}) and BDNF (20 ng ml^{-1}) (Peprotech), and 0.5% FBS (Invitrogen). Prior to electrophysiology experiments, cells at week 3 of terminal differentiation were switched to BrainPhys medium (StemCell Technologies), and experiments were conducted after a total of 5–6 weeks of differentiation. Our protocol produced 8–15% inhibitory neurons, as monitored by immunocytochemistry with anti-GABA antibody.

Cerebral organoid culture preparation

Differentiation of hiPSCs to generate cerebral organoids was performed using a cerebral organoid kit (StemCell Technologies) and by following the manufacturer's instructions. Embryoid bodies with neuroepithelial buds (newly formed organoids) formed after 10 days of the differentiation protocol were transferred to maturation media for development of cortical-like layers and other more mature phenotypes. The age of the organoids was determined from the day they were placed in maturation medium. By 8 weeks of age, we observed the formation of cortical-like layers. Cerebral organoids were maintained on an orbital shaker until used in experiments.

Electrophysiology and pharmacology

Whole-cell recordings were performed using internal solution (in mM): K-gluconate, 120; KCl, 5; MgCl$_2$, 2; HEPES, 10; EGTA; 10; Mg-ATP, 4; pH 7.4 and mOsm 290. The external solution was Ca^{2+} and Mg^{2+}-free Hank's Balanced Salt Solution (HBSS; GIBCO) with added CaCl$_2$, 2 mM; HEPES, 10 mM; glycine, 20 μM; pH 7.4. All recordings were performed using a Multiclamp 700B amplifier (Molecular Devices) at a data sampling rate of 2 kHz with a Digidata 1440A (Molecular Devices). Voltage-clamp and current-clamp protocols were applied using Clampex v10.6 (Molecular Devices). Preliminary analysis and offline filtering at 500 Hz were achieved using Clampfit v10.6 (Molecular Devices). Agonist-induced currents (glutamate-evoked and GABA-evoked) were recorded by applying agonist via a rapid gravity-flow, local superfusion system with electronically-controlled solenoid valves. In general, recordings were obtained at a holding potential of –70 mV in the nominal absence of extracellular magnesium and in the presence of 20 μM glycine (all chemicals from Sigma) and tetrodotoxin (TTX, 1 μM, Hello Bio) was added to inhibit sodium channels and thus action potential-mediated spontaneous transmission. The internal solution for these recordings was (in mM): CsCl, 135; MgCl$_2$, 2; HEPES, 10; EGTA; 1; Mg-ATP, 4; pH 7.4 and mOsm 290. After obtaining a stable seal for whole-cell recording, NMDAR antagonists (50 μM D-(2R)-amino-5-phosphonovalerate [APV, Tocris], 5–10 μM memantine hydrochloride [Sigma] or 5–10 μM NitroSynapsin [aka YQW-036 or NMI-6979, Panorama Research, Inc., Sunnyvale, CA]) were applied to assess the degree of inhibition of glutamate-evoked currents.

Immunocytochemistry of neuronal cultures and cerebral organoids

For 2D neuronal cultures, cells were fixed with 4% paraformaldehyde (PFA) for 20 min, washed with PBS, and blocked with 3% BSA/0.3% Triton X-100 in PBS for 30 min. Cells were incubated with primary antibody overnight, and the appropriate Alexa Fluor (488, 555,

647) conjugated secondary antibody was used at a 1:1000 dilution. Primary antibodies and dilutions were as follows: Tuj1 (1:200; Abcam, Cat. #ab41489), FOXG1 (1:250; Abcam, Cat. #ab18259), GABA (1:100, Sigma, Cat. #A2052). Cells were counterstained with DAPI (1:500; Invitrogen, Cat. #D1306).

For cerebral organoids, after 2 months of development, cells were fixed in 4% PFA at 4 °C overnight followed by serial incubation in 15% and 30% sucrose/PBS overnight. Fixed organoids were embedded in tissue freezing medium (General Data) and flash frozen with isopentane and liquid nitrogen and stored at −80 °C. Frozen organoids were mounted in optimal cutting temperature (OCT) compound and sectioned at 20-μm in a cryostat. Sections were stained with antibodies to Ctip2 (1:200; Abcam, Cat. #ab18465), Tbr2 (1:300; Abcam, Cat. #ab23345), Nestin (1:200; Abcam, Cat. #ab22035), Tuj1 (1:200; Abcam, Cat. #ab41489), or Aβ peptide (1:2000; BioLegend, Cat. #803001), GABA (1:100, Sigma, Cat. #A2052) and imaged with a Nikon A1 laser scanning confocal fluorescence microscope by an observer blinded to the experimental group.

Calcium Imaging.—Two methods for calcium imaging in neurons were used in these studies.

a)   Fura-2 AM Calcium Imaging.: For quantification of intracellular calcium concentrations, we used the ratiometric dye Fura-2. In brief, hiPSC derived cortical neurons were incubated for 30 min in a loading solution containing HBSS with the following additions: $CaCl_2$, 2 mM; $MgCl_2$, 1 mM; Fura-2 AM (Life Technologies), 5 μM; pluronic acid, 0.05% (Life Technologies); HEPES, 10 mM; pH 7.4. The cells were subsequently washed with Ca/Mg-containing HBSS and incubated at RT for 20 min for de-esterification.

Fura-2–based measurements of intracellular calcium were performed using a Lambda DG4 (Sutter Instruments) with an optimized Fura-2 filter set for the 340/380 nm excitation ratio. Images were collected using a CCD camera on a Zeiss Axiovert 100M microscope with a 63X oil objective; exposure time 100 ms. Images were obtained from randomly selected fields of comparable cell density. For determination of intracellular calcium levels, several regions of interest (ROI) of equal area were analyzed using MetaFluor software (Molecular Devices). Values for Fura-2 AM imaging were calculated as ratios of fluorescence recorded at 340 nm and 380 nm for each ROI.

b)   Fluo-4 AM Calcium Imaging.: For monitoring the relative change in intracellular calcium concentration vs. time at high video-rate resolution, the non-ratiometric dye fluo-4 (Life Technologies) was used to allow for better temporal resolution than possible with fura-2. In brief, hiPSC-derived cortical neurons were incubated for 1 hour at RT in a loading solution containing HBSS plus: $CaCl_2$, 2 mM; $MgCl_2$, 1 mM; fluo-4AM, 8 μM; pluronic acid, 0.05%; HEPES, 10 mM; pH 7.4. The cells were subsequently washed with Ca/Mg-containing HBSS and incubated at RT for 1 hour for de-esterification.

To monitor fluo-4 fluorescence changes, we excited at 480 nm, imaged using a 40X oil objective and analyzed with MetaMorph software (Molecular Devices). The exposure time for recording spontaneous calcium transients was 30 ms, and images were captured

at 33 frames per second. Images were of randomly selected fields of comparable cell density. Changes in intracellular calcium from baseline (F_0) to peak fluorescence (ΔF) were expressed as fractional changes above baseline ($\Delta F/F_0$). Events with $\Delta F/F$ rise times of <500 ms were considered neuronal transients; most of these transients had rise times of 100–200 ms [24]. Neurons could be distinguished from astrocytes morphologically and by their responses to NMDA. To verify this identification, in some cases immunostaining was used for class III β-tubulin (Tuj1) or microtubule associated protein 2 (MAP2) to identify neurons and glial fibrillary associated protein (GFAP) or S100β for astrocytes. To study the contribution of various receptors to spontaneous calcium activity, we applied specific inhibitors: APV for NMDARs, 6,7-dinitroquinoxaline-2,3-dione (DNQX, Hello Bio) for non-NMDARs, and bicuculline (Tocris) for $GABA_ARs$.

Movies of the fluo-4 calcium imaging were prepared at 500 frames per second using ImageJ (NIH).

Oscillatory spectral power analysis

All spectral analyses were performed with custom MATLAB (MathWorks) code. The calcium imaging recordings were acquired at a sampling rate of 33, 50, or 55 Hz, and linearly detrended (detrend.m). Power spectral densities (PSDs) for each dataset were computed using Welch's method (pwelch.m, 10-second window, 8-second overlap), and standardized across recordings by removing (dividing through) the high-frequency 1/f baseline (5–15 Hz). Finally, low-frequency power was computed by summing the log power from 0.2–1 Hz and averaged across groups (WT vs. AD). To compare results pre- and post-NitroSynapsin and bicuculline application, the power ratio was computed at each frequency, and low-frequency power subsequently logged and summed.

Code availability

Custom MATLAB (MathWorks) code used for oscillatory spectral power analysis is available online for public use.

Multielectrode array (MEA) recording

For MEA recordings, cells were plated as described above on CytoView 12 well plates (Axion Biosystems) coated with 0.1% polyethyleneimine (PEI). Experiments were conducted after 5–6 weeks of hiPSC differentiation. For MEA recordings of cerebral organoids, 6-week-old organoids were plated on CytoView 12-well plates coated with 0.1% polyethyleneimine (PEI) and laminin (10 μg/ml). Recordings were performed in BrainPhys medium at 37 °C using the 'neural spikes analog mode' setting with a sampling frequency of 12.5 kHz at baseline (prior to) and after 5 μM NitroSynapsin treatment (Axion Biosystems Maestro Axis Software version 2.4.2) on a Maestro MEA (Axion Biosystems). For firing frequency calculations, an electrode was considered active if it displayed >5 spikes per min. A network burst was characterized by a minimum of 25 electrodes displaying >10 spikes per electrode at an inter-spike interval of <100 ms. Network burst frequency was defined as total number of network bursts divided by duration of analysis expressed in Hz. For determining synchronous firing, windows of 20 ms duration were analyzed. A synchrony window is defined as the window of time around zero that is used to compute the area under

the cross-correlation curve. Synchrony index is defined as a unitless measure of synchrony between 0 and 1 derived from well-wide, pooled interelectrode cross-correlation. Values closer to 1 indicate higher synchrony.

AD transgenic mice

All animal procedures were approved by the IACUC at Sanford Burnham Prebys Medical Discovery Institute, University of California, San Diego, or The Scripps Research Institute. For animal studies, age- and sex-matched mice were randomly chosen and assigned to the various experimental treatment groups. hAPP-J20 mice express a transgene encoding pathogenic human APP (with Swedish and Indiana mutations), producing a high-level of Aβ42 peptide. hAPP-J20 AD mice (or WT littermate controls) were treated with vehicle (V), memantine (M) or NitroSynapsin (N) starting at 90 days of age, a time when they are beginning to display abnormal phenotypes. Initial treatment was an equimolar loading dose (20 mg/kg M; 28 mg/kg N) followed by twice daily equimolar maintenance doses (1 mg/kg M; 1.4 mg/kg N) for 3 months.

Immunohistochemistry of mouse brain

Immunohistochemistry was performed on hAPP-J20 AD mouse brains and compared to WT littermate controls. Brains were fixed in freshly prepared 4% PFA and cut into 40 μm-thick vibratome sections. Immunolabeling was performed using mouse monoclonal antibodies against neuronal-specific proteins: microtubule associated protein 2 (MAP2, 1:100; Millipore) and synaptophysin (1:500; Millipore). After overnight incubation with primary antibody, sections were incubated with Texas red or FITC-conjugated horse anti-mouse IgG secondary antibody (1:75; Vector Laboratories) and mounted with anti-fading media (Vector). Immunosignals were analyzed by quantitative immunofluorescence using blind-coded sections, serially imaged on a laser-scanning confocal microscope, and quantified using NIH Image 1.43 software. At least three sections for each brain and four fields for each section were analyzed in each brain area.

Biotin-switch assay for detection of S-nitrosylated proteins

Five to eight-month-old hAPP-J20 mice were administered intraperitoneal NitroSynapsin (1.4 mg/kg) every 12 hours for 5 days to approximate steady-state [5, 18, 21]. Between 6- to-12 hr after the final injection, the mice were anesthetized and transcardially perfused with saline solution. Mouse brains were then collected, snap-frozen, and stored at −80 °C until assayed. Biotin-switch assay was performed on lysates prepared as previously described [25–27] to detect S-nitrosylation of the NMDAR or off target proteins. S-Nitrosylation of the principal subunit of the NMDAR, GluN1, was detected with subunit-specific antibodies. In brief, brain tissue samples were homogenized in 0.5 mL HEN buffer (100 mM Hepes pH 7.2, 1 mM EDTA, 0.1 mM neocuproine) with 1% Triton X-100 and 0.1% SDS. A total of 500 μg of protein per sample was used for the assay. Free thiol groups were blocked by incubation with 2 mM S-methyl methanethiosulfonate (Millipore-Sigma) for 20 min at 42°C. Cell extracts were then precipitated with acetone and resuspended in HEN buffer with 1% SDS. S-Nitrosothiol groups were then selectively reduced with 50 mM ascorbate to free thiols, which were subsequently biotinylated with 1 mM biotin HPDP WS (Dojindo Molecular Technologies). The biotinylated proteins were pulled down

with high-capacity NeutrAvidin-agarose beads (Thermo Fisher Scientific) and analyzed by immunoblotting. Total and S-nitrosylated (SNO-)GluN1 were detected with anti-GluN1 antibody (Cell Signaling Technology, rabbit monoclonal Cat #5704). For quantification of immunoblots, images were scanned with a LICOR Odyssey CLx imaging system. Total protein as a loading control was also quantified by standard immunoblot analysis. Results were expressed as the ratio of SNO-GluN1 to total GluN1 protein.

Data analysis and statistics

We used 3–5 independent sets of neuronal cultures from separate differentiations and 4 independent groups of cerebral organoids from separate differentiations for patch clamp, calcium imaging, and MEA recordings. Sample size was determined from prior power analyses based on prior data obtained in our laboratory. All data was acquired by an investigator blinded to the sample groups. Data are presented as mean ± SEM. Statistical analyses were performed using GraphPad Prism software. Statistical significance was determined by a two-tailed unpaired Student's t-test for single comparisons, by a two-tailed ANOVA followed by a post-hoc test for multiple comparisons, or by a Sidak's test corrected for multiple comparisons between selected pairs. Statistical significance was determined by one-sample t-test for comparison of the mean log power before vs. after application of bicuculline; this test was run separately for WT and AD neurons. A p value < 0.05 was considered to be statistically significant. In general, the variance was similar between groups being compared. No samples or data were excluded from the analysis.

Results

NitroSynapsin abrogates AD neuronal hyperexcitability

We studied AD hiPSC-derived cerebrocortical neuronal cultures with one allele bearing the PS1 ΔE9 mutation (ΔE9/WT), PS1M146V mutation (M146V/WT), or APP^{swe} mutation (APP^{swe}/WT) vs. WT/WT isogenic controls. Within 5 weeks of culture and continuing thereafter, AD hiPSC-derived neurons displayed the forebrain marker, FOXG1 (Supplementary Fig. 1a). In addition to excitatory neurons, our hiPSC-derived neuronal cultures contained 5–10% GABAergic interneurons (Supplementary Fig. 1b). We first investigated neuronal excitability at the single-cell level during patch-clamp recordings and found a 2–3-fold increase in the frequency of spontaneous action potentials in AD neurons compared to WT isogenic controls (Fig. 1a, b, Supplementary Fig. 2a, b). Notably, the majority of neurons reported in this study were excitatory based on the fact that very few neurons stained positively with anti-GABA antibody (Supplementary Fig. 1b).

Considering ligand-gated currents, we found glutamate-evoked current density in whole-cell recordings to be ~2.5-fold greater in AD neurons versus WT (Fig. 1c, d, Supplementary Fig. 2c, d). A maximally effective concentration of the NMDAR antagonist APV (50 μM) inhibited 75–80% of the glutamate-induced current in both PS1 mutant AD neurons and in WT isogenic neurons (Supplementary Fig. 2e, f). However, the improved eNMDAR antagonist NitroSynapsin (e.g., at 10 μM) blocked 50–80% but only ~20% of the AD mutant and WT isogenic currents, respectively (Fig. 1e, f, Supplementary Fig. 2g, h). The NMDAR antagonist approved by the FDA for treatment of AD, memantine (at 5 or 10

μM), manifested a significantly smaller effect than NitroSynapsin at blocking the increased glutamatergic currents manifested by AD mutant neurons (Fig. 1e, f, Supplementary Fig. 2g, h). These drug concentrations were chosen from our previously published dose-response curves for both memantine and NitroSynapsin, which found that the 10 μM concentration was maximally potent for each, with NitroSynapsin manifesting greater efficacy, i.e., reaching greater percent inhibition [5, 18–20, 28–30]. As we had demonstrated previously, an important feature of both of these uncompetitive aminoadamantane NMDAR open-channel blockers is their ability to relatively spare smaller/physiological glutamatergic currents (e.g., phasic synaptic activity), while inhibiting larger/pathological responses (e.g., tonic extrasynaptic activity) [5, 17, 19, 20, 26, 31, 32]. Accordingly, in contrast to their effect on AD neurons, in the present study we observed only a minor degree of blockade of the smaller, glutamate-induced currents of the WT isogenic neurons treated with memantine or NitroSynapsin (Fig. 1e, f, Supplementary Fig. 2g, h).

We also observed a decrease in the magnitude of maximal GABA-evoked currents in AD neurons compared to WT isogenic neurons (Supplementary Fig. 2i, j). This is in agreement with prior studies reporting decreased GABA-evoked currents in membranes from AD human brains due to loss of functional $GABA_A$ receptors [33].

Aberrant glutamate-related responses monitored with Ca^{2+} imaging

Similar to glutamate-evoked current responses, using the calcium indicator fluo-4, we observed a 2.5-fold increase in glutamate-evoked Ca^{2+} levels in AD neurons compared to WT isogenic controls (Fig. 2a, b, Supplementary Fig. 3a, b). To permit better estimates of absolute intracellular calcium levels $[Ca^{2+}]_i$ during the resting state, we used the ratiometric calcium indicator fura-2, and found significantly higher basal $[Ca^{2+}]_i$ in AD hiPSC neurons and in contiguous astrocytes than in their WT isogenic control cultures (Fig. 2c, d, Supplementary Fig. 3c, d). We had previously shown that exogenously applied $A\beta_{42}$ oligomers increased $[Ca^{2+}]_i$ in WT neurons and astrocytes [5]. Thus, the known increase in $A\beta_{42}$ in our AD hiPSC cultures [22, 23] may account for the elevated basal $[Ca^{2+}]_i$ that we observed here. Moreover, recent studies using calcium imaging on mouse brain also reported an increase in basal activity after application of human Aβ dimers [34], providing in vivo validation for our approach with hiPSC-based models.

Additionally, AD hiPSC-derived neuronal cell bodies displayed a 2–3-fold increase in spontaneous Ca^{2+} transients compared to WT neurons. In this case, we monitored calcium with fluo-4, which was used instead of fura-2 to enhance temporal resolution of the signal (Fig. 2e, f, Supplementary Fig. 3e, f, Supplementary Movies 1 and 2). One possible explanation for the elevated calcium levels under these conditions is Aβ-induced inhibition of glutamate re-uptake or increased release from astrocytes as well as neurons, which in turn promotes hyperactivity in the neurons, as discussed previously [4, 5, 29, 34, 35]. In support of aberrant glutamate release, we found that application of 50 nM tetanus toxin [36], which is known to inhibit vesicular release, abrogated the increase in spontaneous calcium transient activity in PS1 mutant AD hiPSC neuronal cultures (Supplementary Fig. 3g, h). The preventive action of tetanus toxin also indicates that the observed aberrant activity did not occur merely because of agonal glutamate release, for example during cell

death, reinforcing the fact that this aberrant activity represents a true pathophysiological phenotype of the mutant AD cells. We also found that 1 μM TTX could significantly inhibit spontaneous calcium transients in both AD and WT neuronal cultures, suggesting that the calcium responses were dependent, at least in part, on the spontaneous, sodium channel-mediated action potentials in the neuronal network (Supplementary Fig. 4a, b).

In addition to NMDARs, AMPA receptors (AMPARs) are also implicated in the pathogenesis of AD [37, 38]. Therefore, to ascertain the contribution of AMPARs in the aberrant activity of AD cultures, we treated our AD and WT cultures with 20 μM DNQX, a non-NMDAR antagonist. DNQX significantly inhibited the calcium responses in both AD and WT cultures, suggesting that AMPARs play a role in mediating this neuronal activity (Supplementary Fig. 4c–e). However, the decrease in both calcium transient frequency and intracellular calcium levels was significantly greater with maximally-effective concentrations of APV than with DNQX in the AD neurons, suggesting a greater contribution of NMDARs than AMPARs to the pathological hyperactivity observed in AD (Supplementary Fig. 4c–e). AMPARs may be important, for example, to glutamate-mediated depolarization of the neuronal membrane, thus relieving Mg^{2+} block of NMDARs to allow calcium entry via their receptor-operated channels.

NitroSynapsin normalizes calcium network signaling in AD hiPSC-derived neurons

Compared to equimolar memantine, we found that NitroSynapsin abrogated to a significantly greater degree not only the spontaneous bursts of calcium transients, but also the increased basal neuronal calcium levels in AD cultures (Fig. 3a–e, Supplementary Movie 2). In contrast to the effect of these drugs on AD neurons, we found no significant difference between basal calcium levels in WT neurons before or after exposure to either 5 μM NitroSynapsin or equimolar memantine (Fig. 3a–e, Supplementary Movie 1).

Analysis of the power spectrum of the spontaneous calcium transients revealed bursts of low frequency events (<1 Hz) in both WT and AD cultures (Fig. 3f). Additionally, in a subset of the cultures, we observed theta (~6 Hz) oscillations (Fig. 3f), which are known to arise spontaneously in both normal and AD human brains [13]. Such spontaneous synchronous events are known to reflect dynamic excitatory/inhibitory (E/I) balance in the network and contribute to very slow oscillations that constitute the default activity pattern of the cortical network observed in vivo [39, 40]. The peaks of spontaneous calcium transients in actively firing neurons coincide with the 'up-state' of these slow oscillations, and the silent troughs coincide with the 'down-state.' Greater spontaneous calcium transients would mean up-state elongation and down-state shortening, potentially causing network dysfunction and contributing to dynamic E/I imbalance [39, 40]. We found significantly greater power (corresponding to amplitude) of spontaneous calcium transients in the 0.2–1 Hz range in hiPSC-derived AD cultures, indicative of a disrupted and hyperexcitable cortical network (Fig. 3f, g). Of potential therapeutic importance in correcting E/I imbalance, application of 5 μM NitroSynapsin reduced the low frequency power to a far greater degree in AD cultures than in WT (Fig. 3h).

Next, we studied the contribution of inhibitory neurons to the low frequency power in AD cultures. Interestingly, we did not find a change in the low frequency power in AD

cultures in the presence of 50 μM bicuculline (BIC, a selective $GABA_A$ receptor antagonist). Nonetheless, BIC did significantly increase the low frequency power in WT cultures, suggesting a greater role of inhibitory neurons under WT conditions (Supplementary Fig. 4f, i). Accordingly, although BIC significantly increased the calcium transient frequency and intracellular calcium levels in AD neurons, the increase was much greater in WT neurons (Supplementary Fig. 4f–h), consistent with the recently-reported decrease in inhibitory drive in AD mutant hAPP knock-in mice compared to WT [41].

NitroSynapsin corrects hypersynchrony in AD neurons and cerebral organoids

Interestingly, we also observed hypersynchronous burst activity among neurons at the network level in AD cultures during multielectrode array (MEA) recordings. In AD cultures compared to WT, network burst synchrony, frequency, and mean firing rate within a burst were all significantly increased 2–8 fold (Fig. 4a–f). Such synchrony has previously been attributed, at least in part, to astrocytic release of glutamate [42, 43], which occurs in response to Aβ oligomer exposure [5]. NitroSynapsin decreased this aberrant activity in a concentration-dependent manner (Fig. 4a–f, Supplementary Fig. 5a–e). Importantly, NitroSynapsin (5 μM) normalized the dramatically increased firing frequency, network burst frequency and synchrony of AD cultures to a level similar to that of WT cultures (Fig. 4a–f, Supplementary Fig. 5a–e). Moreover, treatment with 5 μM NitroSynapsin manifested no significant effect on spike rate or network activity in the WT cultures (Fig. 4a, d–f, Supplementary Fig. 5a–e).

Additionally, we studied AD-related hyperactivity in M146V/WT, APP^{swe}/WT, and WT/WT hiPSC-derived 3D cerebral organoids. These organoids manifested reproducible cortical-like layer formation and contained mature GABAergic interneurons under our conditions (Fig. 5a, Supplementary Fig. 6b). We found an increase in Aβ immunostaining, and electrical activity in AD organoids compared to WT (Fig. 5b, c, Supplementary Fig. 6a). Similar to our 2D cultures, AD organoids showed increased network burst frequency and firing synchrony compared to WT (Fig. 5b, e, f). Conventional NMDAR blockers like APV prevented the hyperactivity, showing that it is caused by dysregulation of NMDA-type glutamate receptors (Supplementary Fig.7); NitroSynapsin (10 μM) normalized the excessive mean firing rate, network burst frequency, and firing synchrony of the AD organoids, while having minimal effect on WT organoids (Fig. 5b–f). In contrast, equimolar memantine was not effective in decreasing the hyperactivity (Fig. 5b–f).

NitroSynapsin rescues dendritic circuits and synaptic damage in mouse AD models in vivo while targeting the nitro group to the NMDAR

Previously, we had reported that NitroSynapsin at similar micromolar concentrations can protect synapses, preserve plasticity circuits, and improve memory in the triple transgenic AD mouse model (3xTg-AD), which harbors the PS1M146V, APP^{Swe}, and tau(P301L) transgenes [5, 44]. Since in the current study we used hiPSC-derived AD neuronal cultures manifesting increased Aβ [12], we wanted to test the effect of NitroSynapsin in a transgenic mouse model with similar findings, e.g., with genetic alteration in hAPP alone. Thus, we used hAPP-J20 AD mice, which bear the APP^{swe}/APP^{ind} transgenes [45] and are known to display excessive excitability [46]. We found that treatment with NitroSynapsin protected

dendritic networks and presynaptic endings in the hAPP-J20 AD mice (Supplementary Fig. 8a–d). These data are consistent with our previous findings that, mechanistically, this damage is predominantly due to excessive NMDAR activity [5].

Aminoadamantanes are known to inhibit excessive NMDAR activity via uncompetitive, open-channel block. Additionally, we previously reported that NitroSynapsin target a nitro group to redox-active/inhibitory sites on the NMDAR via a chemical reaction known as S-nitrosylation, while avoiding off-target nitrosylation [26]. To prove targeting empirically in AD transgenic mice, we performed biotin-switch assays to assess the presence of an 'NO group' on GluN1, the principal subunit of the NMDAR, in hAPP-J20 mouse brain after treatment with NitroSynapsin. Notably, diseases associated with increased RNS, such as AD transgenic mice, would be expected to show somewhat increased nitrosylation of the NMDAR compared to WT littermate controls, and we found that to be the case here. Importantly, however, treatment with NitroSynapsin significantly increased S-nitrosylation of the NMDAR over basal levels, and this effect lasted at least 6–12 hours after the last dose of drug (Supplementary Fig 8e, f).

Discussion

hiPSC-derived neurons/organoids model hyperactivity in human AD

Although in vitro systems cannot be expected to simulate all of the complex characteristics of a neurodegenerative disorder such as AD, we reasoned that hiPSC models might allow us to study aspects of the electrical properties of AD neurons in a human context. The fact that our cultures manifest complex in vivo neural network properties similar to those recently reported in living mouse models of oligomeric Aβ-induced activity [34] gave us confidence that the system might faithfully recapitulate at least some of the features of the disease state. Additionally, after differentiating the hiPSC-derived neurons for ~5 weeks, they showed stable, mature phenotypes, allowing us to examine early aspects of the disease in the cells that bear AD-causing mutations. Moreover, after >2 months of maturation, our WT and AD cerebral organoids manifested cortical-like layer formation, contained both excitatory and inhibitory neurons, and displayed neural network properties that allowed us to probe the etiology and potential treatment of the hyperexcitability observed early in the pathogenesis of AD. In particular, we were interested in studying electrophysiological and synaptic dysfunction that might occur prior to the synapse loss, which represents the hallmark of more advanced stages of AD. In this regard, our hiPSC AD models yielded results in concordance with EEG findings in human AD patients. Thus, our findings potentially yield insight into the origin and potential treatment of the observed hyperexcitable phenotype that occurs in both human AD patients and our hiPSC model system.

NitroSynapsin ameliorates hyperexcitability

Hyperexcitability and the involvement of glutamate receptor dysfunction have been implicated in the pathophysiology of AD in prior studies on a variety of animal and cell-based models [5, 9, 34, 46, 47]. Mechanistically, for example, Aβ oligomers have been shown to enhance neuronal NMDAR responses and to inhibit glutamate re-uptake by astrocytes [35, 48, 49], which would result in larger glutamate-evoked currents in AD

cultures compared to WT controls, as observed here. Moreover, positive clinical trials with the NMDAR antagonist memantine provided additional evidence for NMDAR hyperactivity in the AD brain that contributes to symptoms [18, 50]. However, a critical question in the field is whether targeting NMDARs might be sufficient for a disease-modifying therapy (i.e., a drug that can reverse synapse loss and behavioral/cognitive abnormalities). If treatment with improved NMDAR antagonists could achieve this level of protection, it would mean that prior drugs like memantine were simply not sufficiently efficacious.

The new, more effective NMDAR antagonist, NitroSynapsin, manifests dual-allosteric inhibitory action -- in addition to blocking excessively open NMDAR-associated ion channels like memantine, it also provides targeted S-nitrosylation of NMDARs [26]. S-Nitrosylation of the NMDAR represents a physiological negative-feedback system to limit excessive ion influx through the receptor [51]. In the presence of excessive NMDAR activity, generating increased levels of NO, the receptor subunits display some degree of protein S-nitrosylation (see, for example, [26] in the setting of cerebrovascular disease). However, the degree of protein S-nitrosylation is not maximal even under pathological circumstances, so further increasing the percentage of S-nitrosylated NMDARs can offer additional inhibition of the receptors. NitroSynapsin works by augmenting the targeting of NO to the NMDAR, as evidenced in biotin-switch blots for S-nitrosylated proteins after NitroSynapsin treatment; this redox modification appears to result in channel desensitization. Moreover, we have shown in our previous studies that excessive activity of extrasynaptic (e)NMDARs (as opposed to synaptic receptors) in AD leads to pathologically increased NO production in neurons, which in turn contributes to a modest but significant increase in S-nitrosylation of the NMDAR [52, 53]. Collectively, the redox effect mediated by protein S-nitrosylation added to the open-channel block of NitroSynapsin leads to more effective inhibition of the NMDARs than memantine, which only provides open-channel block of the NMDAR. Furthermore, inhibition by memantine can be relieved by depolarization of the neuron, as occurs with increasing pathological insult, whereas the inhibitor effect of protein S-nitrosylation of the NMDAR is not relieved by depolarization since the affected redox sites are outside of the membrane voltage field [51].

While prior studies on mouse transgenic AD models suggest that NitroSynapsin, might be capable of rescuing synapses and cognitive behavioral deficits to reverse the disease process, results in AD mouse models have been notoriously unreliable in predicting human clinical outcomes [53, 54]. Thus, the shortcomings of current AD mouse models mandate that additional model systems, such as hiPSC-based models, are necessary for the purpose of screening potential drugs for human clinical trials.

Neurons derived from hiPSCs bearing human AD-related mutations show many of the molecular markers of the disease [22, 23]. To date, however, there have been no detailed functional studies of their electrophysiology. Here, we show that AD hiPSC-derived cerebrocortical neurons exhibit hyperexcitability phenotypes similar to those observed in human AD patients [9, 16]. The AD hiPSC neurons we used exhibit high basal levels of intracellular calcium and increased spontaneous activity compared to WT isogenic controls. Spontaneous resting state activity (0.2 – 1 Hz) has been widely used to evaluate brain network properties [39]. Recently, this hyperexcitable state has been associated with non-

convulsive epileptic events and decreased cognition in humans with AD [16]. Understanding the mechanism(s) contributing to this hyperactivity could possibly lead to the development of better treatment regimens. In our AD hiPSC neuronal model system, NitroSynapsin normalized these aberrant spontaneous electrical events to a significantly greater extent than by memantine, while leaving the properties of WT neurons, which manifest smaller currents, relatively unaffected. These results suggest that NitroSynapsin may be more effective than memantine as a human AD drug with similar clinical tolerability. Moreover, this study establishes the feasibility of using patient-derived hiPSC neuronal cultures and cerebral organoids as electrophysiological models of neuronal plasticity in which neuronal networks can be studied and used for screening novel therapeutic compounds.

Supplementary Material

Refer to Web version on PubMed Central for supplementary material.

Acknowledgments:

References

1. Palop JJ, Mucke L. Epilepsy and cognitive impairments in Alzheimer disease. Arch Neurol 2009; 66(4): 435–440. [PubMed: 19204149]

2. Palop JJ, Mucke L. Network abnormalities and interneuron dysfunction in Alzheimer disease. Nat Rev Neurosci 2016; 17(12): 777–792. [PubMed: 27829687]

3. Tu S, Okamoto S, Lipton SA, Xu H. Oligomeric Aβ-induced synaptic dysfunction in Alzheimer's disease. Mol Neurodegener 2014; 9: 48. [PubMed: 25394486]

4. Abramov E, Dolev I, Fogel H, Ciccotosto GD, Ruff E, Slutsky I. Amyloid-β as a positive endogenous regulator of release probability at hippocampal synapses. Nat Neurosci 2009; 12(12): 1567–1576. [PubMed: 19935655]

5. Talantova M, Sanz-Blasco S, Zhang X, Xia P, Akhtar MW, Okamoto S et al. Aβ induces astrocytic glutamate release, extrasynaptic NMDA receptor activation, and synaptic loss. Proc Natl Acad Sci USA 2013; 110(27): E2518–2527. [PubMed: 23776240]

6. Quiroz YT, Budson AE, Celone K, Ruiz A, Newmark R, Castrillon G et al. Hippocampal hyperactivation in presymptomatic familial Alzheimer's disease. Ann Neurol 2010; 68(6): 865–875. [PubMed: 21194156]

7. Nygaard HB, Kaufman AC, Sekine-Konno T, Huh LL, Going H, Feldman SJ et al. Brivaracetam, but not ethosuximide, reverses memory impairments in an Alzheimer's disease mouse model. Alzheimers Res Ther 2015; 7(1): 25. [PubMed: 25945128]

8. Verret L, Mann EO, Hang GB, Barth AM, Cobos I, Ho K et al. Inhibitory interneuron deficit links altered network activity and cognitive dysfunction in Alzheimer model. Cell 2012; 149(3): 708–721. [PubMed: 22541439]

9. Vossel KA, Beagle AJ, Rabinovici GD, Shu H, Lee SE, Naasan G et al. Seizures and epileptiform activity in the early stages of Alzheimer disease. JAMA Neurol 2013; 70(9): 1158–1166. [PubMed: 23835471]

10. Israel MA, Yuan SH, Bardy C, Reyna SM, Mu Y, Herrera C et al. Probing sporadic and familial Alzheimer's disease using induced pluripotent stem cells. Nature 2012; 482(7384): 216–220. [PubMed: 22278060]

11. Drummond E, Wisniewski T. Alzheimer's disease: experimental models and reality. Acta Neuropathol 2017; 133(2): 155–175. [PubMed: 28025715]

12. Ghatak S, Dolatabadi N, Trudler D, Zhang X, Wu Y, Mohata M et al. Mechanisms of hyperexcitability in Alzheimer's disease hiPSC-derived neurons and cerebral organoids vs. isogenic control. eLife 2019; 8.

13. Zhang H, Watrous AJ, Patel A, Jacobs J. Theta and Alpha Oscillations Are Traveling Waves in the Human Neocortex. Neuron 2018; 98(6): 1269–1281 e1264. [PubMed: 29887341]

14. Liu X, Wang S, Zhang X, Wang Z, Tian X, He Y. Abnormal amplitude of low-frequency fluctuations of intrinsic brain activity in Alzheimer's disease. J Alzheimers Dis 2014; 40(2): 387–397. [PubMed: 24473186]

15. Ferrazzoli D, Albanese M, Sica F, Romigi A, Sancesario G, Marciani MG et al. Electroencephalography and dementia: a literature review and future perspectives. CNS Neurol Disord Drug Targets 2013; 12(4): 512–519. [PubMed: 23574167]

16. Lam AD, Deck G, Goldman A, Eskandar EN, Noebels J, Cole AJ. Silent hippocampal seizures and spikes identified by foramen ovale electrodes in Alzheimer's disease. Nat Med 2017; 23(6): 678–680. [PubMed: 28459436]

17. Li S, Jin M, Koeglsperger T, Shepardson NE, Shankar GM, Selkoe DJ. Soluble Aβ oligomers inhibit long-term potentiation through a mechanism involving excessive activation of extrasynaptic NR2B-containing NMDA receptors. J Neurosci 2011; 31(18): 6627–6638. [PubMed: 21543591]

18. Lipton SA. Paradigm shift in neuroprotection by NMDA receptor blockade: memantine and beyond. Nat Rev Drug Discov 2006; 5(2): 160–170. [PubMed: 16424917]

19. Chen H-SV, Pellegrini JW, Aggarwal SK, Lei SZ, Warach S, Jensen FE et al. Open-channel block of *N*-methyl-d-aspartate (NMDA) responses by memantine: therapeutic advantage against NMDA receptor-mediated neurotoxicity. J Neurosci 1992; 12(11): 4427–4436. [PubMed: 1432103]

20. Chen H-SV, Lipton SA. Mechanism of memantine block of NMDA-activated channels in rat retinal ganglion cells: uncompetitive antagonism. J Physiol (Lond) 1997; 499 (Pt 1): 27–46. [PubMed: 9061638]

21. Wang Y, Eu J, Washburn M, Gong T, Chen H-SV, James WL et al. The pharmacology of aminoadamantane nitrates. Curr Alzheimer Res 2006; 3(3): 201–204. [PubMed: 16842096]

22. Paquet D, Kwart D, Chen A, Sproul A, Jacob S, Teo S et al. Efficient introduction of specific homozygous and heterozygous mutations using CRISPR/Cas9. Nature 2016; 533(7601): 125–129. [PubMed: 27120160]

23. Woodruff G, Young JE, Martinez FJ, Buen F, Gore A, Kinaga J et al. The presenilin-1 E9 mutation results in reduced γ-secretase activity, but not total loss of PS1 function, in isogenic human stem cells. Cell Rep 2013; 5(4): 974–985. [PubMed: 24239350]

24. Winship IR, Plaa N, Murphy TH. Rapid astrocyte calcium signals correlate with neuronal activity and onset of the hemodynamic response in vivo. J Neurosci 2007; 27(23): 6268–6272. [PubMed: 17554000]

25. Jaffrey SR, Erdjument-Bromage H, Ferris CD, Tempst P, Snyder SH. Protein S-nitrosylation: a physiological signal for neuronal nitric oxide. Nat Cell Biol 2001; 3(2): 193–197. [PubMed: 11175752]

26. Takahashi H, Xia P, Cui J, Talantova M, Bodhinathan K, Li W et al. Pharmacologically targeted NMDA receptor antagonism by NitroMemantine for cerebrovascular disease. Sci Rep 2015; 5: 14781. [PubMed: 26477507]

27. Uehara T, Nakamura T, Yao D, Shi ZQ, Gu Z, Ma Y et al. S-nitrosylated protein-disulphide isomerase links protein misfolding to neurodegeneration. Nature 2006; 441(7092): 513–517. [PubMed: 16724068]

28. Tu S, Akhtar MW, Escorihuela RM, Amador-Arjona A, Swarup V, Parker J et al. NitroSynapsin therapy for a mouse MEF2C haploinsufficiency model of human autism. Nat Commun 2017; 8(1): 1488. [PubMed: 29133852]

29. Pirttimaki TM, Codadu NK, Awni A, Pratik P, Nagel DA, Hill EJ et al. α7 Nicotinic receptor-mediated astrocytic gliotransmitter release: Aβ effects in a preclinical Alzheimer's mouse model. PLoS One 2013; 8(11): e81828. [PubMed: 24312364]

30. Okamoto S, Pouladi MA, Talantova M, Yao D, Xia P, Ehrnhoefer DE et al. Balance between synaptic versus extrasynaptic NMDA receptor activity influences inclusions and neurotoxicity of mutant huntingtin. Nat Med 2009; 15(12): 1407–1413. [PubMed: 19915593]

31. Hanson JE, Pare JF, Deng L, Smith Y, Zhou Q. Altered GluN2B NMDA receptor function and synaptic plasticity during early pathology in the PS2APP mouse model of Alzheimer's disease. Neurobiol Dis 2015; 74: 254–262. [PubMed: 25484285]

32. Xia P, Chen HS, Zhang D, Lipton SA. Memantine preferentially blocks extrasynaptic over synaptic NMDA receptor currents in hippocampal autapses. J Neurosci 2010; 30(33): 11246–11250. [PubMed: 20720132]

33. Limon A, Reyes-Ruiz JM, Miledi R. Loss of functional GABA$_A$ receptors in the Alzheimer diseased brain. Proc Natl Acad Sci USA 2012; 109(25): 10071–10076. [PubMed: 22691495]

34. Zott B, Simon MM, Hong W, Unger F, Chen-Engerer HJ, Frosch MP et al. A vicious cycle of β amyloid-dependent neuronal hyperactivation. Science 2019; 365(6453): 559–565. [PubMed: 31395777]

35. Li S, Hong S, Shepardson NE, Walsh DM, Shankar GM, Selkoe D. Soluble oligomers of amyloid β protein facilitate hippocampal long-term depression by disrupting neuronal glutamate uptake. Neuron 2009; 62(6): 788–801. [PubMed: 19555648]

36. Schiavo G, Benfenati F, Poulain B, Rossetto O, Polverino de Laureto P, DasGupta BR et al. Tetanus and botulinum-B neurotoxins block neurotransmitter release by proteolytic cleavage of synaptobrevin. Nature 1992; 359(6398): 832–835. [PubMed: 1331807]

37. Whitcomb DJ, Hogg EL, Regan P, Piers T, Narayan P, Whitehead G et al. Intracellular oligomeric amyloid-β rapidly regulates GluA1 subunit of AMPA receptor in the hippocampus. Sci Rep 2015; 5: 10934. [PubMed: 26055072]

38. Hettinger JC, Lee H, Bu G, Holtzman DM, Cirrito JR. AMPA-ergic regulation of amyloid-β levels in an Alzheimer's disease mouse model. Mol Neurodegener 2018; 13(1): 22. [PubMed: 29764453]

39. Krishnan GP, Gonzalez OC, Bazhenov M. Origin of slow spontaneous resting-state neuronal fluctuations in brain networks. Proc Natl Acad Sci USA 2018; 115(26): 6858–6863. [PubMed: 29884650]

40. Sanchez-Vives MV, Massimini M, Mattia M. Shaping the default activity pattern of the cortical network. Neuron 2017; 94(5): 993–1001. [PubMed: 28595056]

41. Petrache AL, Rajulawalla A, Shi A, Wetzel A, Saito T, Saido TC et al. Aberrant excitatory-inhibitory synaptic mechanisms in entorhinal cortex microcircuits during the pathogenesis of Alzheimer's disease. Cereb Cortex 2019; 29(4): 1834–1850. [PubMed: 30766992]

42. Angulo MC, Kozlov AS, Charpak S, Audinat E. Glutamate released from glial cells synchronizes neuronal activity in the hippocampus. J Neurosci 2004; 24(31): 6920–6927. [PubMed: 15295027]

43. Fellin T, Pascual O, Gobbo S, Pozzan T, Haydon PG, Carmignoto G. Neuronal synchrony mediated by astrocytic glutamate through activation of extrasynaptic NMDA receptors. Neuron 2004; 43(5): 729–743. [PubMed: 15339653]

44. Oddo S, Caccamo A, Shepherd JD, Murphy MP, Golde TE, Kayed R et al. Triple-transgenic model of Alzheimer's disease with plaques and tangles: intracellular Aβ and synaptic dysfunction. Neuron 2003; 39(3): 409–421. [PubMed: 12895417]

45. Mucke L, Masliah E, Yu GQ, Mallory M, Rockenstein EM, Tatsuno G et al. High-level neuronal expression of Aβ$_{1-42}$ in wild-type human amyloid protein precursor transgenic mice: synaptotoxicity without plaque formation. J Neurosci 2000; 20(11): 4050–4058. [PubMed: 10818140]

46. Palop JJ, Chin J, Roberson ED, Wang J, Thwin MT, Bien-Ly N et al. Aberrant excitatory neuronal activity and compensatory remodeling of inhibitory hippocampal circuits in mouse models of Alzheimer's disease. Neuron 2007; 55(5): 697–711. [PubMed: 17785178]

47. Shankar GM, Bloodgood BL, Townsend M, Walsh DM, Selkoe DJ, Sabatini BL. Natural oligomers of the Alzheimer amyloid-β protein induce reversible synapse loss by modulating an NMDA-type

glutamate receptor-dependent signaling pathway. J Neurosci 2007; 27(11): 2866–2875. [PubMed: 17360908]

48. Ferreira IL, Bajouco LM, Mota SI, Auberson YP, Oliveira CR, Rego AC. Amyloid β peptide 1–42 disturbs intracellular calcium homeostasis through activation of GluN2B-containing *N*-methyl-D-aspartate receptors in cortical cultures. Cell Calcium 2012; 51(2): 95–106. [PubMed: 22177709]

49. Matos M, Augusto E, Oliveira CR, Agostinho P. Amyloid-β peptide decreases glutamate uptake in cultured astrocytes: involvement of oxidative stress and mitogen-activated protein kinase cascades. Neuroscience 2008; 156(4): 898–910. [PubMed: 18790019]

50. Reisberg B, Doody R, Stoffler A, Schmitt F, Ferris S, Mobius HJ et al. Memantine in moderate-to-severe Alzheimer's disease. N Engl J Med 2003; 348(14): 1333–1341. [PubMed: 12672860]

51. Choi Y-B, Tenneti L, Le DA, Ortiz J, Bai G, Chen H-SV, Lipton SA. Molecular basis of NMDA receptor-coupled ion channel modulation by S-nitrosylation. Nat Neurosci 2000; 3(1):15–21. [PubMed: 10607390]

52. Molokanova E, Akhtar MW, Sanz-Blasco S, Tu S, Pina-Crespo JC, McKercher SR et al. Differential effects of synaptic and extrasynaptic NMDA receptors on Aβ-induced nitric oxide production in cerebrocortical neurons. J Neurosci 2014; 34(14): 5023–5028. [PubMed: 24695719]

53. Nakamura T, Lipton SA. Protein S-nitrosylation as a therapeutic target for neurodegenerative Diseases. Trends Pharmacol Sci 2016; 37(1): 73–84. [PubMed: 26707925]

54. Hall AM, Roberson ED. Mouse models of Alzheimer's disease. Brain Res Bull 2012; 88(1): 3–12. [PubMed: 22142973]

55. Lehman EJ, Kulnane LS, Gao Y, Petriello MC, Pimpis KM, Younkin L et al. Genetic background regulates β-amyloid precursor protein processing and β-amyloid deposition in the mouse. Hum Mol Genet 2003; 12(22): 2949–2956. [PubMed: 14506131]
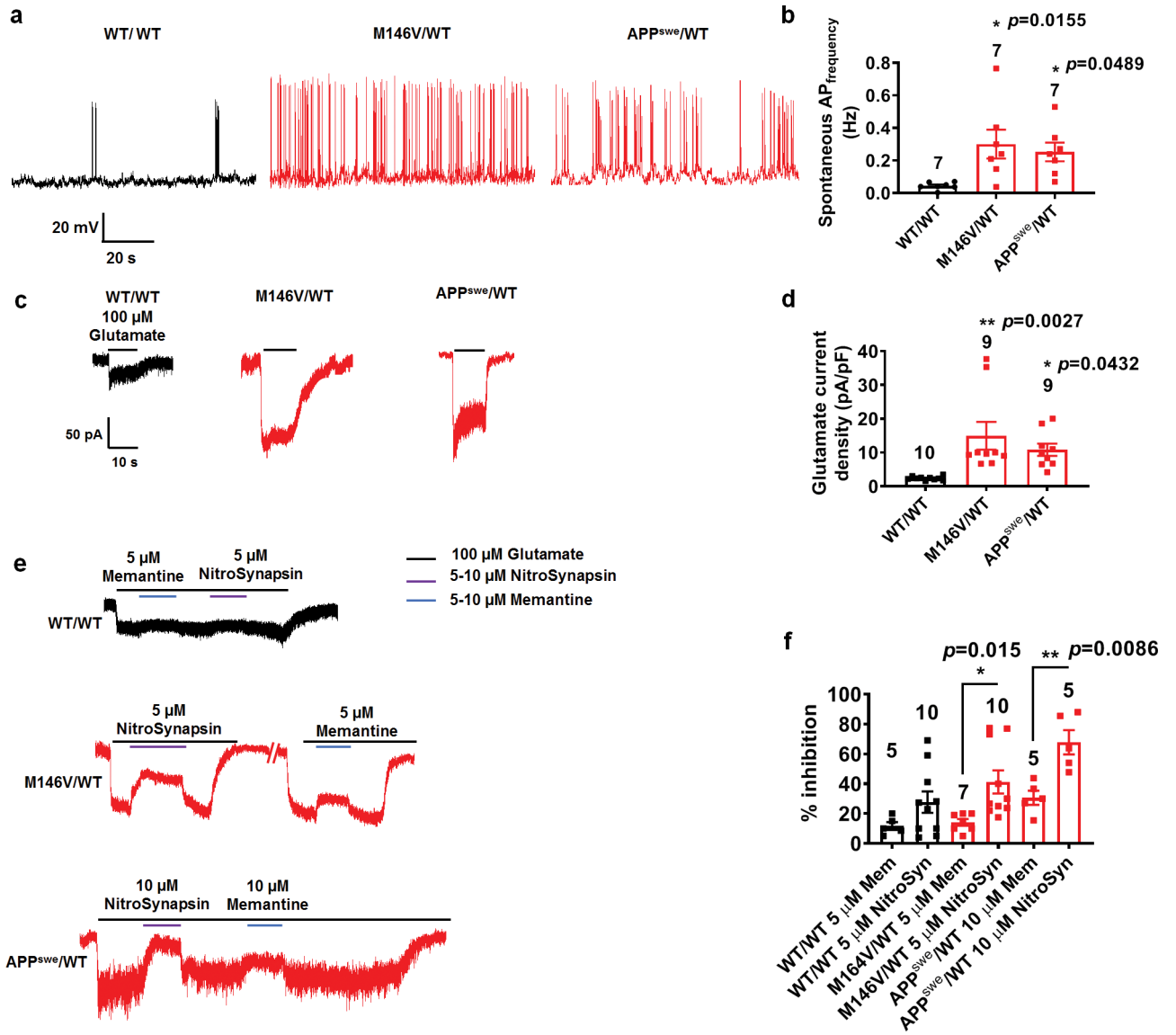
Fig. 1. AD neurons manifest increased spontaneous action potentials and glutamate-evoked currents compared to WT neurons.

a Spontaneous action potentials (sAP) at resting membrane potential (RMP). WT/WT hiPSC-derived cerebrocortical neuron data in black, M146V/WT and APP[swe]/WT in red. **b** Quantification of sAP frequency. **c** Representative traces of glutamate-evoked currents from neurons voltage-clamped at −70 mV. **d** Glutamate-evoked current density. **e**, **f** Inhibition by 5–10 μM memantine or NitroSynapsin. Representative traces of WT/WT, M146V/WT and APP[swe]/WT neurons clamped at −70 mV (e). Percent inhibition by memantine (Mem) or NitroSynapsin (NitroSyn) in M146V/WT and APP[swe]/WT neurons vs. their respective WT/WT isogenic controls (f). Sample size represents total number of neurons recorded and is listed above bars. Data are mean ± SEM. Exact *p* values are listed above bars in this and subsequent figures unless otherwise specified. Statistical significance analyzed by ANOVA with post hoc Dunnett's test.
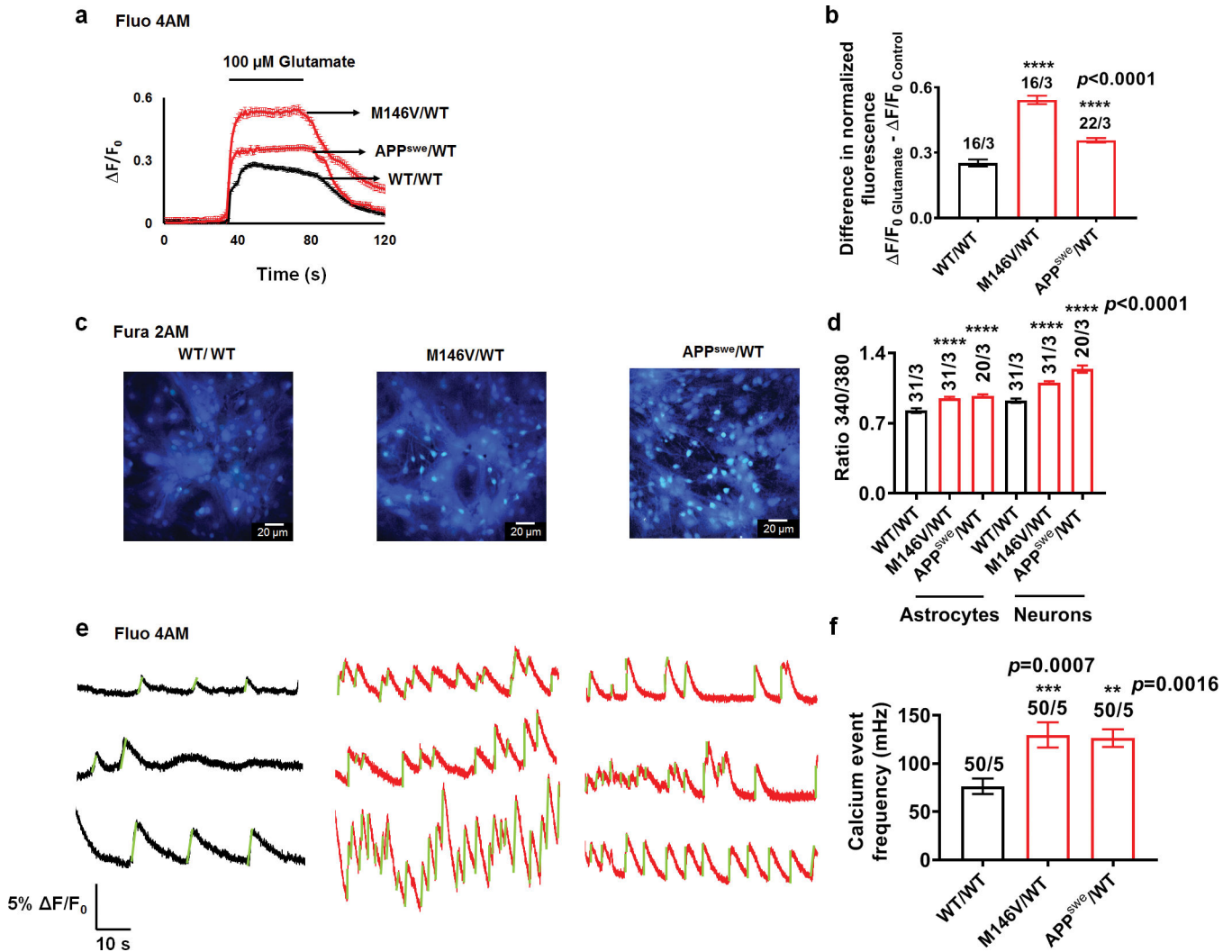
Fig. 2. AD neurons manifest enhanced intracellular calcium levels and spontaneous transients compared to WT isogenic neurons.
a Glutamate evoked calcium responses. Fluo-4 calcium indicator fluorescence over time after exposure to glutamate in M146V/WT, APP^{swe}/WT vs. WT/WT neurons. **b** Quantification of difference in total calcium response to glutamate. **c** Fura-2 340/380 nm ratio images showing representative basal intracellular calcium levels. **d** Quantification of basal [Ca^{2+}]$_i$ in astrocytes and neurons. **e** Spontaneous neuronal calcium transients. Calcium responses recorded from individual neurons loaded with fluo-4 AM. Neuronal calcium transients with rise times <500 ms are highlighted in green. **f** Quantification of calcium transient frequency. Sample size represents total number of cells analyzed/total number of independent experiments. Data are mean ± SEM. Each cell was considered separate data point. Statistical significance was analyzed by ANOVA with post hoc Dunnett's test.
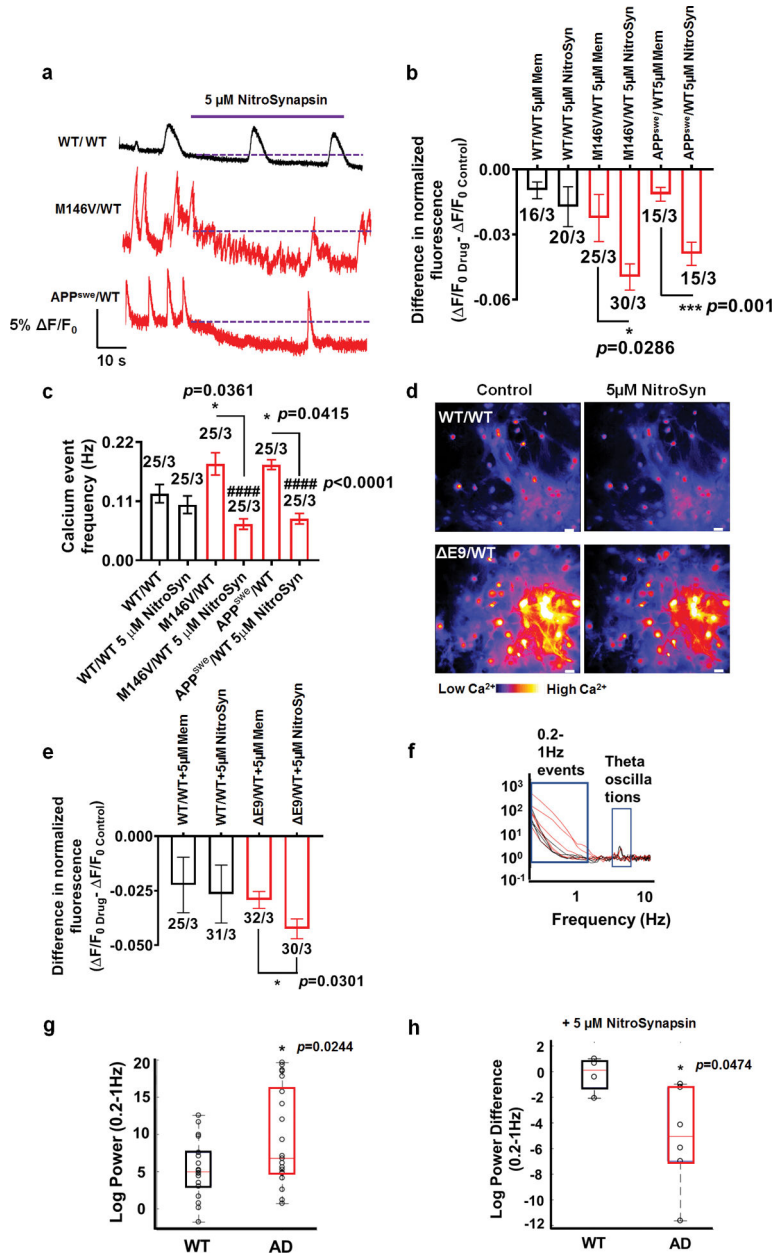
Fig. 3. NitroSynapsin inhibits spontaneous calcium activity and 0.2–1 Hz events in AD neurons.
WT/WT hiPSC-derived cerebrocortical neuron data in black, M146V/WT and APP[swe]/WT
in red. **a** Representative calcium imaging traces showing decrease in $[Ca^{2+}]_i$ and
transients after application of 5 μM NitroSynapsin. Dotted line represents decrease
in $[Ca^{2+}]_i$. **b** Quantification of difference in normalized fluorescence ($\Delta F/F_{0Drug}$ - $\Delta F/F_{0Control}$) in response to 5 μM memantine (Mem) or equimolar NitroSynapsin (NitroSyn).
c Quantification of calcium event frequency before and after application of 5 μM
NitroSynapsin. **d** Fluo-4 images of WT/WT and ΔE9/WT cultures showing $[Ca^{2+}]_i$ before
(control) and after application of NitroSynapsin (5 μM NitroSyn). Scale bar: 10 μm.
e Quantification of difference in normalized fluorescence ($\Delta F/F_{0Drug}$ - $\Delta F/F_{0Control}$) in
response to 5 μM memantine (Mem) or equimolar NitroSynapsin (NitroSyn). **f** Noise-floor

normalized power spectrum showing concentration of power in low frequencies (<1 Hz) and at 6 Hz (theta oscillation). WT in black; AD in red. **g** Quantification of mean log power (0.2–1 Hz) in WT and AD cultures. **h** Quantification of mean log power difference (0.2–1 Hz) after treatment with 5 μM NitroSynapsin in WT and AD cultures (post - pre). Data are mean ± SEM. Statistical significance analyzed by two-tailed unpaired Student's t-test (*) in b, e, g and h; by ANOVA with post hoc Dunnett's test (*) for multiple comparisons to WT; and by Sidak's test (#) corrected for multiple comparisons between selected pairs in c.
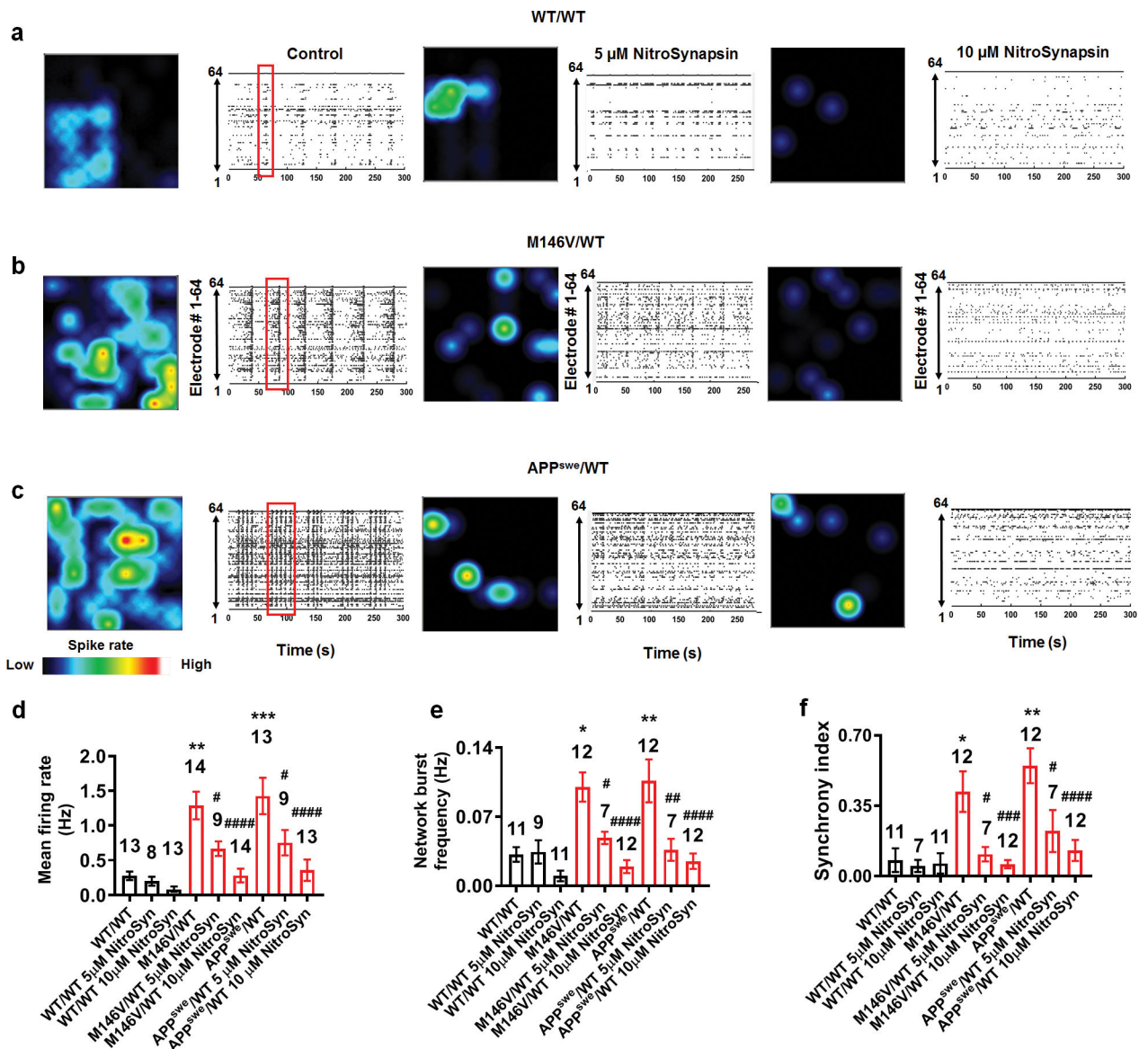
Fig. 4. NitroSynapsin decreases network burst frequency, synchrony, and firing rate in AD neurons in a concentration-dependent manner.

a-c Representative heat maps and raster plots of MEA recordings in WT/WT (a), M146V/WT (b), and APP^{swe}/WT (c) cultures before (*left*) and after (*center and right*) treatment with 5 and 10 μM NitroSynapsin, respectively. Red boxes represent examples of network bursts. **d-f** Quantification of MEA recordings. Mean firing rate (d). Network burst frequency quantification (e). Quantification of synchrony index (f). Data are mean ± SEM. Sample size listed above bar graphs (*,$^{\#}$$p < 0.05$; **,$^{\#\#}$$p < 0.01$; ***,$^{\#\#\#}$$p < 0.001$; $^{\#\#\#\#}$$p < 0.0001$ by ANOVA with post-hoc Dunnett's test (*) for multiple comparisons to WT and Sidak's test ($^{\#}$) corrected for multiple comparisons between selected pairs).
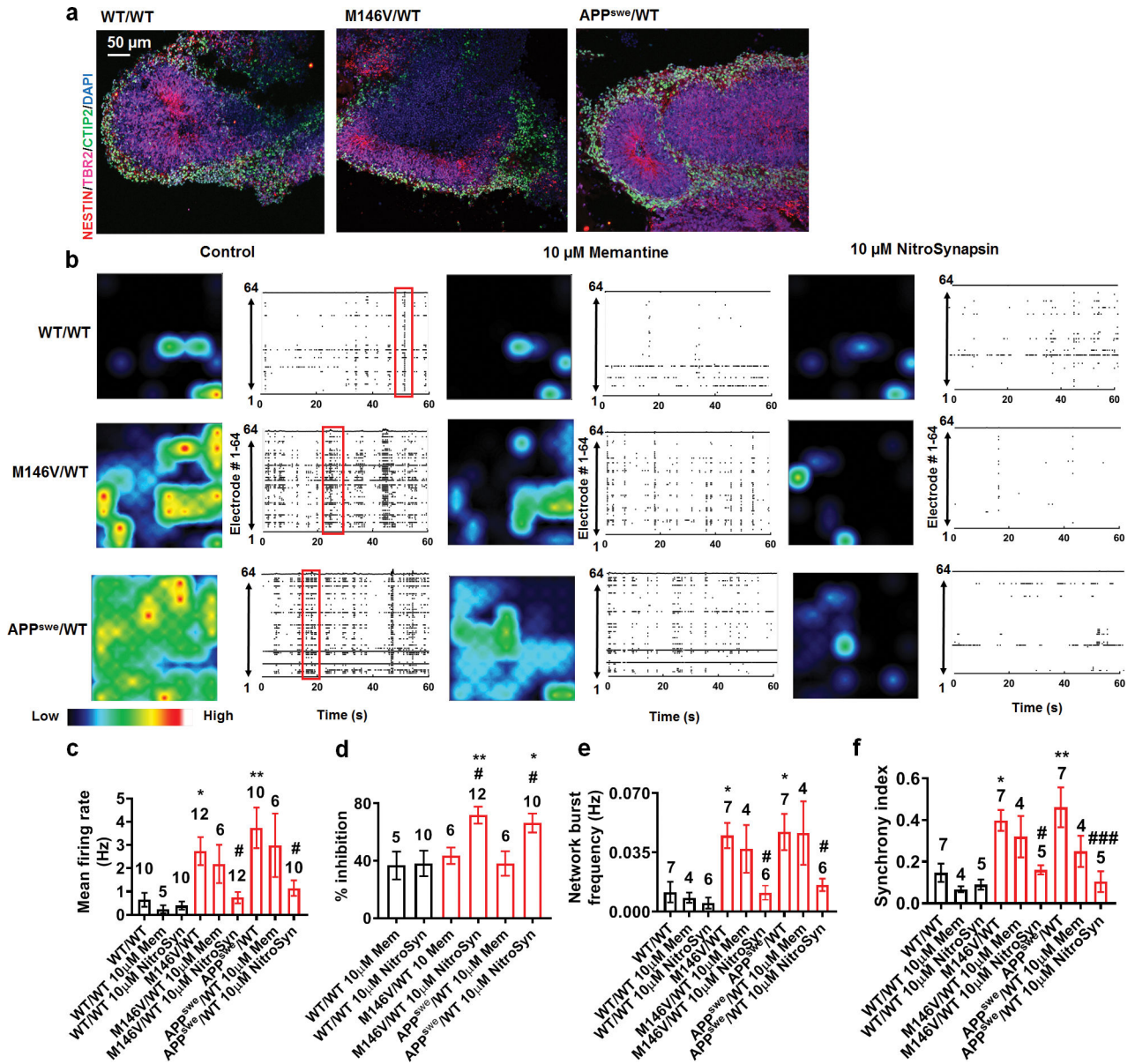
Fig. 5. AD cerebral organoids show hypersynchronous burst activity compared to WT.
a Representative images of 2-month old WT/WT, M146V/WT, and APP[swe]/WT organoids
stained for Nestin, TBR2, and CTIP2 showing cortical layers. **b** Representative raster plots
of MEA recordings in 3-month old WT/WT, M146V/WT, and APP[swe]/WT organoids before
(left) and after treatment with 10 μM memantine (center) or 10 μM NitroSynapsin (right).
Red boxes represent examples of network bursts. **c-f** Quantification of MEA recordings.
Mean firing rate; percentage inhibition with 10 μM memantine or NitroSynapsin; network
burst frequency, and synchrony index. Data are mean ± SEM. Sample size listed in the bar
graphs (*,#$p < 0.05$; **,##$p < 0.01$ by ANOVA with post-hoc Dunnett's test (*) for multiple
comparisons to WT and Sidak's test (#) corrected for multiple comparisons between selected
pairs).